Journal of Molecular Spectroscopy 381 (2021) 111533

Contents lists available at ScienceDirect

Journal of Molecular Spectroscopy

journal homepage: www.elsevier.com/locate/yjmsp

High resolution threshold photoelectron spectrum and autoionization processes of S_2 up to 15.0 eV

Helgi Rafn Hrodmarsson [a,1,*], Gustavo A. Garcia [a], Laurent Nahon [a], Jean-Christophe Loison [b], Bérenger Gans [c]

[a] Synchrotron SOLEIL, L'Orme des Merisiers, St Aubin, BP 48, Gif sur Yvette, France
[b] ISM, Université Bordeaux 1, CNRS, 351 cours de la Libération, 33405, Talence Cedex, France
[c] Institut des Sciences Moléculaires d'Orsay, CNRS, Université Paris-Saclay, 91405, Orsay, France

ARTICLE INFO

Keywords:
S_2 diradical
Photoelectron spectroscopy
i^2PEPICO
Total ion yield
VUV photoionization

ABSTRACT

VUV photoionization dynamics of the S_2 molecule were re-investigated from threshold up to 15.0 eV, using synchrotron radiation coupled with double imaging photoelectron/photoion coincidence featuring high resolution capabilities. We measured the first threshold photoelectron spectrum of S_2 achieving higher resolution than previous literature to derive accurate spectroscopic constants for a few electronic states of the cation including the $X^2\Pi_{\Omega,g}$ ground state and the $a^4\Pi_u$, $b^4\Sigma_g^-$, and $B^2\Sigma_g^-$ states. We also recorded the total ion yield for S_2 up to a photon energy of 15.0 eV which, combined with the threshold photoelectron spectrum, led to the assignment of various autoionizing Rydberg series.

1. Introduction

Sulfur and its chemistry are not only an integral component of biochemical processes[1] but are omnipresent in the interstellar medium as well [2]. Neutral S_2 has been found in cometary comae [3,4], on Jupiter near the G impact site after the collision of Shoemaker-Levy 9 [5], in volcanic plumes on Io [6,7], and has been invoked as a contributor to stratospheric heating of hot Jupiters [8]. However, somewhat intriguingly, in primitive molecular clouds and star-forming regions, sulfur is increasingly depleted [9,10]. An abundance of sulfur-bearing molecules has been detected recently in the interstellar medium [11–15], but all-together it does not sufficiently account for the apparently missing sulfur. A theory gaining traction presumes that sulfur collects on interstellar dust grains where it is processed by UV and X-rays to form universal sulfur sinks such as S_8 [16]. In this context it is important to revisit the photoionization of the sulfur dimer, S_2, as it is a potentially important reactive intermediate in interstellar regions whose chemistry is driven by UV and X-ray radiation.

Since the recording of the first photoelectron spectra of the S_2 diradical [17,18], the spectroscopy of the S_2^+ cation has been explored by means of flowing afterglow [19–21], electron impact ionization [22], optical spectroscopy [23], photoluminescence in Ne matrices [24], and absorption spectroscopy of sulfur-doped silica glass [25]. The photoionization efficiency (PIE) curve of S_2 was measured up to 20.7 eV by Liao and Ng [26] and theoretical efforts pertaining to the ground state and excited states of the S_2^+ radical have been recently summarized [27]. Experimental efforts to study breakdown products from the interaction of disulfide bridge-containing molecules with high energy photons found that S_2^+ was persistently formed at energies in the low-keV regime, attesting its chemical stability [28].

The work of Rosinger *et al.*[22], revealed several features in the recorded ionization efficiency curves which were attributed to autoionization processes, and Liao and Ng [26] further inspected these autoionizing features which had clearly visible bands in the PIE curve of S_2. While they noted that it was likely that these vibrational bands could be grouped into more than one vibrational progression, only a handful were assigned.

By using the double-imaging photoelectron/photoion coincidence (i^2PEPICO) technique [29] coupled with synchrotron radiation we present the threshold photoelectron spectra (TPES) and total ion yield (TIY) from threshold up to 15.0 eV. The TIY allows us to assign features corresponding to autoionization of neutral Rydberg states converging to different vibronic states of S_2^+, which are in turn assigned using the TPES. We also present a two-dimensional kinetic energy *vs* photon energy matrix of the cation signal which further evidences these ionization dynamics.

* Corresponding author at: Niels Bohrweg 2, 2333CA Leiden. the Netherlands.
[1] Current address: Laboratory for Astrophysics, Leiden Observatory, Leiden University, PO Box 9513, NL-2300 RA, Leiden, the Netherlands.

https://doi.org/10.1016/j.jms.2021.111533
Received 2 August 2021; Received in revised form 6 September 2021; Accepted 10 September 2021
Available online 29 September 2021

2. Methodologies

Experiments were performed on the DESIRS VUV undulator beamline [30] located at the third generation French national synchrotron facility SOLEIL. The experimental apparatus that was used is the permanent molecular beam end-station SAPHIRS [31] which is equipped with the i^{2}PEPICO spectrometer DELICIOUS3 [32]. Ions and electrons were detected in coincidence with an imaging Wiley-McLaren time-of-flight analyzer and a velocity map imaging (VMI) setup, respectively. The DESIRS beamline monochromator was set to deliver a photon energy resolution of 3 meV at 8 eV and a gas filter [33] upstream was filled with either krypton or argon depending on the energy range, to filter out higher harmonics of the beamline undulator, OPHELIE2 [34].

S_2 was produced by recombination of S atoms which were formed by double H-abstraction from H_2S in a flow-tube placed inside the SAPHIRS chamber [35]. The S_2 diradicals were produced as secondary products of a process initially set up to produce SH radicals. All the experimental parameters pertaining to this experiment have been described in detail previously [36].

Three energy scans were performed; one from threshold up to 12.0 eV and two scans from 11.9 eV to 15.0 eV, one in which the particle acceleration was achieved with a DC electric field of 53 V•cm^{-1} and one where it was increased to 177 V•cm^{-1} to collect all coincident events related to S_2^+ ions up to 15 eV. Autoionizing resonances corresponding to transitions in neutral atomic sulfur were used for absolute photon energy calibration. This does not account for the Stark shift in the recorded TPES which is induced by the applied DC electric field to achieve particle acceleration. The Stark shift can be quantified by calculating $6\sqrt{F}$ (in cm^{-1} with F denoting the electric field in V•cm^{-1}) [29] which gives a shift of 5.4 meV in the case of the 53 V•cm^{-1} scans that were used to record the TPES. All the ionization thresholds given in this paper have been corrected by this field-induced shift.

At each photon energy of the scans, the recorded images were inversed [37] so the electron signal detected in coincidence with $^{32}S_2$ can be obtained as a function of electron kinetic energy and photon energy in a two-dimensional matrix representation (see below). Therein, diagonal signals correspond to direct ionizations into a cationic state where the kinetic energy of the produced photoelectrons increases linearly with excess energy. Vertical lines, however, evidence excitations to Rydberg states that are resonant with the photon energy, which autoionize according to the different couplings to the cation states.

The threshold photoelectron spectrum (TPES) is obtained by integrating the intensities along the diagonal lines (constant ionic states) up to a relatively small value of kinetic energy [38,39]. For this experiment, the best signal to background ratio was found for an electron kinetic energy cut-off (Ele KE$_{max}$) value of 5 meV.

Mass signals corresponding to m/z = 65 ($^{33}S^{32}S$) and m/z = 66 ($^{34}S^{32}S$, the $^{33}S_2$ contribution is negligible) were clearly visible [36] and the TPES from these mass channels are analyzed for the $X^2\Pi_{\Omega,g}$ ground state. As for the excited ionic states, the observed peak positions in the recorded TPES are indistinguishable in all mass channels which forbids any differentiation in the analysis of the ionic states of $^{33}S^{32}S$ and $^{34}S^{32}S$, and in $^{32}S_2$. Furthermore, as the $^{33}S^{32}S$ and $^{34}S^{32}S$ signals were significantly weaker than that of the m/z = 64 channel, their TPES were created with larger Ele KE$_{max}$ values, namely 10 meV which also results in larger errors of their spectroscopic parameters as will be discussed in Section 3.2.

3. Results and discussion

3.1. Valence electron configurations of S_2 and S_2^+

Photoionization of homonuclear chalcogens (O_2, S_2, etc.) gives rise to multiplex photodynamics which can be attributed to the nature of being open shell triplet molecular systems. Here we present the electron configurations of the neutral and ionized S_2 to assist the reader through the assignments of the total ion yield curve (Section 3.2) and the TPES (Section 3.3).

The electron configuration of neutral S_2 in the ground state ($X^3\Sigma_g^-$) is the following:

$$[S_2] : (\sigma_{3s})^2(\sigma_{3s}{}^*)^2(\sigma_{3p})^2(\pi_{3p})^4(\pi_{3p}{}^*)^2$$

and for the ground state ($X^2\Pi_{\Omega,g}$) of the S_2^+ cation, the electron configuration is obtained by removing an electron from the $\pi_{3p}{}^*$ orbital:

$$[S_2^+] : (\sigma_{3s})^2(\sigma_{3s}{}^*)^2(\sigma_{3p})^2(\pi_{3p})^4(\pi_{3p}{}^*)$$

The first two excited states of the S_2^+ cation, namely $a^4\Pi_u$ and $A^2\Pi_u$, are obtained by removing an electron from the π_{3p} orbital, spin down and spin up, respectively. As seen in Table 1, four different Rydberg series converging to each of the $a^4\Pi_u$ and $A^2\Pi_u$ states are obtained by promoting an electron from a p orbital, to either s (σ_g) or d (σ_g, π_g, δ_g) Rydberg orbitals.

We note that the approximate quantum defects in the Rydberg series of free atomic sulfur are $\delta = 2.0$ for ns, 1.6 for np, and 0.3 for nd orbitals [40] so that it is not unreasonable to expect similar trends for S_2 as has been done previously [26].

The next two excited states of S_2^+ are $b^4\Sigma_g^-$ and $B^2\Sigma_g^-$. Their electron configurations result from removing an electron from the σ_{3p} orbital, spin down and spin up respectively, meaning that the Rydberg states converging to the b/B states require promoting an electron from a σ binding p orbital and thus, the Rydberg states converging to the $b^4\Sigma_g^-$ & $B^2\Sigma_g^-$ states can have two possible electron configurations (Table 1).

Apart from the cationic states presented in Table 1, there are several other states that have been predicted by Yu *et al.* [27], namely, $1^6\Sigma_u^+$, $1^4\Sigma_g^+$, $1^2\Sigma_u^+$, $1^4\Pi_g$, $1^2\Sigma_g^+$, $1^4\Delta_g$, $1^6\Pi_g$, $1^6\Sigma_g^+$, $1^4\Sigma_u^+$, $1^4\Delta_u$, $2^4\Pi_u$, $1^4\Sigma_u^-$, and $2^4\Pi_g$. The spectroscopic parameters of these states were calculated with onsets ranging from 31854 cm^{-1} (3.9 eV) to 50531 cm^{-1} (6.3 eV) above the $X^2\Pi_{\Omega,g}$ ground state, i.e., above the $B^2\Sigma_g^-$ state.

3.2. Total ion yield

The 2D matrices displaying the mass-filtered electron–ion coincidence signals pertaining to m/z = 64 are presented in Fig. 1. In the first scan from 9.2 to 12.0 eV, the $X^2\Pi_{\Omega,g}$ is the ground state and the first excited state, $a^4\Pi_u$, is seen with an onset of 11.58 eV. The second scan which covers 11.9–15.0 eV, unravels three additional excited states, namely $A^2\Pi_u$, $b^4\Sigma_g^-$, and $B^2\Sigma_g$.

The 2D matrix in the upper panel of Fig. 1 exhibits clear signs of autoionizing resonances that contribute to the ionization signals pertaining to the parent. These appear as vertical lines in the 2D matrix

Table 1
Summary of the valence electron configurations of the cationic states of S_2^+ and the Rydberg states of the neutral S_2 that converge to them.

S_2^+	S_2
Ground state – $X^2\Pi_{\Omega,g}(\Omega = 1/2, 3/2)$:	Ground state – $X^3\Sigma_g^-$:
$(\sigma_{3s})^2(\sigma_{3s}{}^*)^2(\sigma_{3p})^2(\pi_{3p})^4(\pi_{3p}{}^*)$	$(\sigma_{3s})^2(\sigma_{3s}{}^*)^2(\sigma_{3p})^2(\pi_{3p})^4(\pi_{3p}{}^*)^2$
$a^4\Pi_u$ state:	$(\sigma_{3s})^2(\sigma_{3s}{}^*)^2(\sigma_{3p})^2(\pi_{3p})^3(\pi_{3p}{}^*)^2n s\sigma_g$
$(\sigma_{3s})^2(\sigma_{3s}{}^*)^2(\sigma_{3p})^2(\pi_{3p})^3(\pi_{3p}{}^*)^2$	$(\sigma_{3s})^2(\sigma_{3s}{}^*)^2(\sigma_{3p})^2(\pi_{3p})^3(\pi_{3p}{}^*)^2n d\sigma_g$
	$(\sigma_{3s})^2(\sigma_{3s}{}^*)^2(\sigma_{3p})^2(\pi_{3p})^3(\pi_{3p}{}^*)^2n d\delta_g$
	$(\sigma_{3s})^2(\sigma_{3s}{}^*)^2(\sigma_{3p})^2(\pi_{3p})^3(\pi_{3p}{}^*)^2n d\pi_g$
$A^2\Pi_u$ state:	$(\sigma_{3s})^2(\sigma_{3s}{}^*)^2(\sigma_{3p})^2(\pi_{3p})^3(\pi_{3p}{}^*)^2n s\sigma_g$
$(\sigma_{3s})^2(\sigma_{3s}{}^*)^2(\sigma_{3p})^2(\pi_{3p})^3(\pi_{3p}{}^*)^2$	$(\sigma_{3s})^2(\sigma_{3s}{}^*)^2(\sigma_{3p})^2(\pi_{3p})^3(\pi_{3p}{}^*)^2n d\sigma_g$
	$(\sigma_{3s})^2(\sigma_{3s}{}^*)^2(\sigma_{3p})^2(\pi_{3p})^3(\pi_{3p}{}^*)^2n d\delta_g$
	$(\sigma_{3s})^2(\sigma_{3s}{}^*)^2(\sigma_{3p})^2(\pi_{3p})^3(\pi_{3p}{}^*)^2n d\pi_g$
$b^4\Sigma_g^-$ state: Ω	$(\sigma_{3s})^2(\sigma_{3s}{}^*)^2(\sigma_{3p})(\pi_{3p})^4(\pi_{3p}{}^*)^2n p\sigma_u$
$(\sigma_{3s})^2(\sigma_{3s}{}^*)^2(\sigma_{3p})\ (\pi_{3p})^4(\pi_{3p}{}^*)^2$	$(\sigma_{3s})^2(\sigma_{3s}{}^*)^2(\sigma_{3p})(\pi_{3p})^4(\pi_{3p}{}^*)^2n p\pi_u$
$B^2\Sigma_g^-$ state:	$(\sigma_{3s})^2(\sigma_{3s}{}^*)^2(\sigma_{3p})(\pi_{3p})^4(\pi_{3p}{}^*)^2n p\sigma_u$
$(\sigma_{3s})^2(\sigma_{3s}{}^*)^2(\sigma_{3p})\ (\pi_{3p})^4(\pi_{3p}{}^*)^2$	$(\sigma_{3s})^2(\sigma_{3s}{}^*)^2(\sigma_{3p})(\pi_{3p})^4(\pi_{3p}{}^*)^2n p\pi_u$

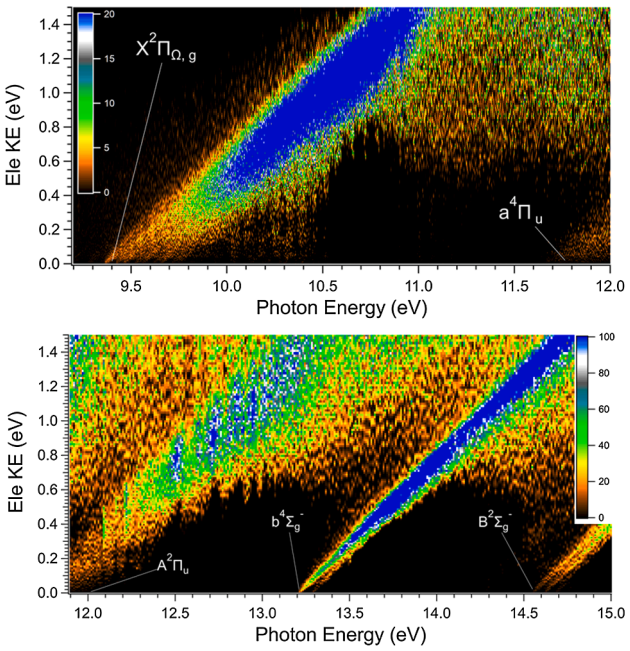

Fig. 1. 2D matrices presenting the relative number of counts of electron–ion coincidences as a function of electron kinetic energy (*y*-axis) and the photon energy (*x*-axis). The upper panel presents the scan from 9.3 to 12.0 eV. The lower panel presents the scan from 11.9 to 15.0 eV. The adiabatic ionization energies for the first five ionic states are presented and discussed in Section 3.3.

whereas direct ionization is observed as diagonal lines. Between 10.0 and 10.5 eV, vertical lines are apparent in the 2D matrix. Above 10.5 eV, these signals seem to partly continue as tendrils dangling down from the direct ionization signal, whose shape resembles that of a diagonal cloud. Around 11.0 eV, the vertical lines become apparent again, albeit very weakly.

The sum of all of the ionic signals as a function of the photon energy in Fig. 1 gives the total ion yield. The first attempt at assigning the autoionizing features in the rich total ion yield of S_2 was made by Liao & Ng [26]. They assigned two Rydberg series converging to the $b^4\Sigma_g^-$ state with average quantum defects of 1.64 and 2.13 which would correspond to the $[b^4\Sigma_g^-]np\pi_u$ and $[b^4\Sigma_g^-]np\ \sigma_u$ Rydberg series, respectively, as outlined in Section 3.1. They observed a plethora of other spectral structures but ultimately, their resolution forbade further assignments despite identifying structures relevant to Rydberg series converging to the ionic states of S_2^+.

Here, the recorded TPES (see Section 3.3) can be used to guide the assignments and identify vibrational features in autoionizing Rydberg series converging to the corresponding ionic states.

Our total ion yield curve along with all of the relevant assignments is shown in Fig. 2 and Table 2 presents the assignments of the onsets of the Rydberg series detailed in Fig. 2 along with the calculated quantum defects which are representative of the Rydberg assignments. Assignments labeled with an asterisk in Table 2 (*) denote blended lines whose energy is best estimated from the calculated quantum defect. The most notable is that of the $[A^2\Pi_u]ns\sigma_g$ Rydberg series whose n = 5–8 components are all blended with other series and hence their assignment should be regarded as tentative despite the quantum defects being comparable.

Sharp dips in the TIY are observed at 10.03 and 10.64 eV which correspond to krypton absorption lines $(4p^5 4s(3/2)_1^\circ \leftarrow 4p^6\ {}^1S_0$ and $4p^5 4s'(1/2)_1^\circ \leftarrow 4p^6\ {}^1S_0$ series, respectively [41]). For the scan up to 12 eV, krypton was used in the gas filter that was used to filter out higher harmonics coming from the undulator. Argon was used in the gas filter for the second scan up to 15 eV which is evidenced by several argon absorption lines, perhaps the most obvious one at 14.30 eV $(3p^1 3d'(3/2)_1^\circ \leftarrow 3p^6\ {}^1S_0$ [42]).

The assignments made by Liao & Ng to the two Rydberg series converging to the $b^4\Sigma^-$ state principally occurred in the spectral region above 12.0 eV. Our assignment completely reevaluates their assignment for two notable reasons. Firstly, the enhanced resolution allows us to observe more structures in the TIY. Secondly, the recorded TPES allows us to more accurately determine the appearance energies of the ionic states than in the PES study of S_2 by Dyke *et al.* [17] (Section 3.3). This greatly influences the calculation of the quantum defects which we used

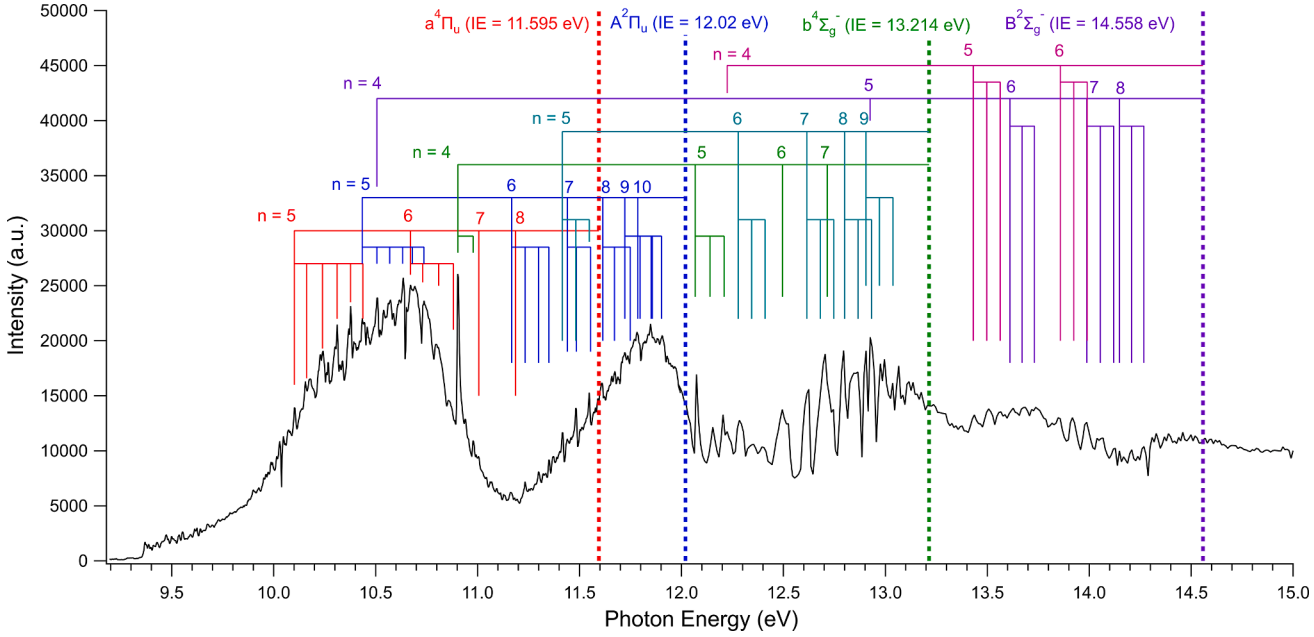

Fig. 2. Total ion yield curve in the photon energy range from 9.2 eV up to 15.0 eV. Different Rydberg series (see Table 1) converging to ionic states are color-coded. The Rydberg series converging to the $a^4\Pi_u$ state is presented in red, the $A^2\Pi_u$ state is presented in blue, the two Rydberg series converging to the $b^4\Sigma_g^-$ state are in green and teal, and the two Rydberg series converging to the $B^2\Sigma_g^-$ state are presented in purple and violet. In most cases we identify more than one vibrational component in the assigned Rydberg series whose vibrational spacing are of the same order as the ionic states assigned in the TPES (see Section 3.3).

Table 2
Rydberg series of S_2 observed in the region 9.2 – 15.0 eV. Blended lines or tentative assignments are denoted with an asterisk. We estimate that the uncertainty of other lines is equal or better than 10 meV. Due to the broadened nature of the autoionizing lines, greater accuracy cannot be expected in this case. Below each Rydberg series we present the corresponding average quantum defect.

Energy		Principal quantum number	Experimentaly-determined Quantum defect	Assignment
eV	cm^{-1}	n	δ	
10.096	81431	5	1.99	$[a^4\Pi_u]5s\sigma_g$
10.666	86028	6	2.17	$[a^4\Pi_u]6s\sigma_g$
11.00*	88730	7	2.21	$[a^4\Pi_u]7s\sigma_g$
11.18*	90182	8	2.27	$[a^4\Pi_u]8s\sigma_g$
Average $\delta = 2.16 \pm 0.12$				
10.43*	84116	5	2.08	$[A^2\Pi_u]5s\sigma_g$
11.16*	90028	6	2.02	$[A^2\Pi_u]6s\sigma_g$
11.48*	92569	7	1.99	$[A^2\Pi_u]7s\sigma_g$
11.64*	93900	8	2.00	$[A^2\Pi_u]8s\sigma_g$
11.741	94698	9	2.02	$[A^2\Pi_u]9s\sigma_g$
11.806	95222	10	2.02	$[A^2\Pi_u]$ $10s\sigma_g$
Average $\delta = 2.02 \pm 0.03$				
10.898	87899	4	1.58	$[b^4\Sigma_g^-]4p\pi_u$
12.062	97287	5	1.56	$[b^4\Sigma_g^-]5p\pi_u$
12.500	100819	6	1.63	$[b^4\Sigma_g^-]6p\pi_u$
12.74*	102755	7	1.64	$[b^4\Sigma_g^-]7p\pi_u$
Average $\delta = 1.60 \pm 0.04$				
11.411	92037	5	2.25	$[b^4\Sigma_g^-]4p\sigma_u$
12.273	98988	6	2.20	$[b^4\Sigma_g^-]5p\sigma_u$
12.610	101707	7	2.25	$[b^4\Sigma_g^-]6p\sigma_u$
12.800	103239	8	2.27	$[b^4\Sigma_g^-]7p\sigma_u$
12.921	104215	9	2.19	$[b^4\Sigma_g^-]8p\sigma_u$
Average $\delta = 2.23 \pm 0.04$				
10.50*	84,697	4	2.17	$[B^2\Sigma_g^-]$ $4p\sigma_u$
12.90*	104,046	5	2.14	$[B^2\Sigma_g^-]$ $5p\sigma_u$
13.606	109,740	6	2.22	$[B^2\Sigma_g^-]$ $6p\sigma_u$
13.983	112,780	7	2.14	$[B^2\Sigma_g^-]$ $7p\sigma_u$
14.143	114,071	8	2.27	$[B^2\Sigma_g^-]$ $8p\sigma_u$
Average $\delta = 2.19 \pm 0.06$				
12.224*	98,594	4	1.59	$[B^2\Sigma_g^-]4p\pi_u$
13.431	108,329	5	1.53	$[B^2\Sigma_g^-]5p\pi_u$
13.858	111,773	6	1.59	$[B^2\Sigma_g^-]6p\pi_u$
Average δ 1.58 ± 0.04				

to guide our assignment to best fit with the recorded TIY.

Though densely populated, we identify a number of Rydberg states in the spectral region between 10 and 11 eV. First of which is the vibrational progression of the $[a^4\Pi_u]5s\sigma_g$ and $[a^4\Pi_u]6s\sigma_g$ states which have a very similar structure and vibrational profile as that of the $a^4\Pi_u$ state. Higher components of the $[a^4\Pi_u]ns\sigma_g$ states can be identified but they are significantly weaker.

The $[a^4\Pi_u]4s\sigma_g$ and $[A^2\Pi_u]4s\sigma_g$ states are not observed in our total ion yield curve and if we use the average quantum defects of both of these series ($\delta = 2.16 \pm 0.12$ and 2.02 ± 0.03, respectively), we can estimate the appearence energies of both components. This would lead the $[a^4\Pi_u]4s\sigma_g$ state to appear between 7.00 and 8.05 eV (56500–64900 cm^{-1}) and the $[A^2\Pi_u]4s\sigma_g$ state between 8.44 and 8.65 eV (68100–69800 cm^{-1}), well below the S_2 ionizaion energy located at ~9.37 eV. These energies are significantly higher than the B and B″ states of S_2 [43] and the closest assignment (to our knowledge) of assigned Rydberg states in this region for S_2 pertain to the $C^3\Sigma^-$ Rydberg state but it was theorized by Cooper & Western that a quintet ion-pair state with an $a^4\Pi_u$ ion core should lie around 72620 cm^{-1} [43]. For the moment, the whereabouts of the $n = 4$ components of the $[a^4\Pi_u]ns\sigma_g$ and $[A^2\Pi_u]ns\sigma_g$ Rydberg series remain up for discussion.

There are some Rydberg series that have been intentionally left out of the assignment which are those of the three Rydberg series corresponding to an excitation to a d Rydberg orbital, namely $[a^4\Pi_u]nd\sigma_g$, $[a^4\Pi_u]nd\delta_g$, $[a^4\Pi_u]nd\pi_g$, $[A^2\Pi_u]nd\sigma_g$, $[A^2\Pi_u]nd\delta_g$, $[A^2\Pi_u]nd\pi_g$.

The quantum defect of d Rydberg-type orbitals are expected to be generally quite small as the quantum defect of such orbitals for atomic sulfur was around 0.3. These states would thus have expected onsets between 9.73 and 10.08 eV in the case of $[a^4\Pi_u]3d\sigma_g$, $[a^4\Pi_u]3d\delta_g$, and $[a^4\Pi_u]3d\pi_g$, and 10.15 and 10.51 eV in the case of $[A^2\Pi_u]3d\sigma_g$, $[A^2\Pi_u]3d\delta_g$, $[A^2\Pi_u]3d\pi_g$. The 9.73 – 10.08 eV region in the TIY does exhibit some structure, but it is too weak for a definitive assignment of the onsets of the $[a^4\Pi_u]3d\ \sigma_g$, $[a^4\Pi_u]3d\delta_g$, and $[a^4\Pi_u]3d\pi_g$ states. The 10.15 – 10.51 eV region on the other hand coincides with the vibrational progression of the $[a^4\Pi_u]5s\sigma_g$ state, which forbids any further assignment of the d Rydberg series.

3.3. Threshold photoelectron spectrum (TPES)

3.3.1. $X^2\Pi_{\Omega,g}$ ground state

The TPES of $^{32}S_2$ is presented in Fig. 3 from its first ionization threshold up to 11.5 eV. The transitions assigned in Fig. 3 are labeled by the final vibrational states of the cation (starting from the neutral S_2 ground state). The TPES of $^{33}S^{32}S$ and $^{34}S^{32}S$ are provided in Fig. S1 of the SI. The vibrational assignments of all isotopologues are given in Table 3.

On average, the observed spin–orbit (SO) splitting in the ground state is 463 ± 17 cm^{-1}. This value compares well with that observed by Dyke *et al.* (470 ± 25 cm^{-1}) [17].

By assigning the vibrational energy levels of the $X^2\Pi_{\Omega,g}$ ground state in the TPES, we can derive the ground state spectroscopic constants, namely T_e, ω_e, and $\omega_e x_e$. To do this, we fit the observed energy levels to obtain the values of T_e, ω_e, and $\omega_e x_e$ that we present in Table 4. We could not include the $\omega_e y_e$ parameter in the fit without degrading the uncertainty of the other parameters.

In Fig. 4 we compare the measured energy level spacing between adjacent spin–orbit ladders of the $X^2\Pi_{\Omega,g}$ ground state and the same energy level spacing using the fitted parameters in Table 3. The agreement is good between $v = 0$–7, but the highest energy levels appear to suffer from perturbation effects from an unknown ionic state. However, since the uncertainties still overlap where the deviation in the energy level spacing is at its greatest, we cannot conclude such a perturbation is present. Furthermore, the additional ionic states predicted by Yu *et al.* [27] would have their onsets at least 32000 cm^{-1} above the onset of the ground state, i.e., around 108000 cm^{-1}, which is still approximately 20000 cm^{-1} higher than the alleged perturbation effects. We can thus not conclude that the ground state is suffering from perturbation effects from a hidden state.

As the TPES of these isotopologues were much weaker than that of $^{32}S_2$, their fitted parameters suffer from larger uncertainties which make any discussion of supposed perturbations mute.

The unassigned peaks at 10.894 eV, 11.005 eV and 11.065 eV from Fig. 3 can now be tentatively assigned by using the derived spectroscopic parameters from the TPES as presented in Table 4. By extrapolating the fitted values to higher v levels, we can tentatively estimate that these peaks belong to the $X^2\Pi_{3/2}(v = 16)$, $X^2\Pi_{1/2}(v = 18)$ and $X^2\Pi_{3/2}(v = 18)$ levels, respectively. This comes with the assumption that these levels are reasonably unperturbed.

Regarding the peak intensities in the $X^2\Pi_{\Omega,g}$ ground state, they do not follow a definite Franck-Condon intensity trend. Between 10.0 and 10.6 eV, rather than decreasing monotonously, the signals increase in intensity before decreasing and disappearing above 10.6 eV. This is due to the presence of autoionizing states that can enhance weak direct transitions by indirect processes, because the vibrational overlap between the intermediate autoionizing state and the final cation state may be

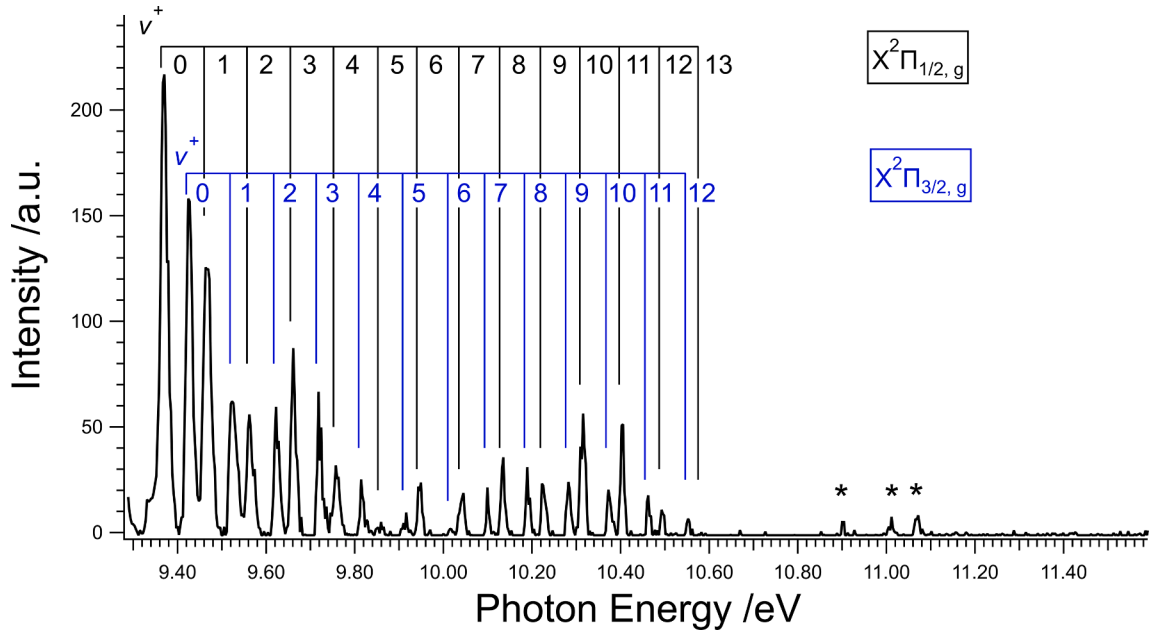

Fig. 3. TPES of $^{32}S_2$. Vibrational assignments of the $X^2\Pi_{\Omega,g}(\Omega = 1/2,3/2)$ground state are presented in black and blue. A few outstanding peaks at 10.894 eV, 11.005 eV and 11.065 eV labeled by asterisks remain unassigned for now.

Table 3
Vibrational and spin–orbit assignments of the final $X^2\Pi_{\Omega,g}v$ ionic states. The values have been corrected by the 5.4 meV Stark shift caused by the electric field (53 V•cm^{-1}). The errors of the peak positions are obtained by convoluting the photon energy accuracy (2 meV) and the pointing accuracy which are on average smaller for $^{32}S_2$ than the $^{33}S^{32}S$ and $^{34}S^{32}S$ isotopologues due to the larger electron bandwidth used to create their TPES and their weaker signal-to-noise ratio.

$\Pi_{\Omega,v}$		Energy $^{32}S_2$		Energy $^{33}S^{32}S$		Energy $^{34}S^{32}S$	
Ω	v	eV	cm^{-1}	eV	cm^{-1}	eV	cm^{-1}
1/2	0	9.371 ± 0.002	75580 ± 16	9.368 ± 0.002	75,560 ± 17	9.369 ± 0.002	75564 ± 16
3/2	0	9.428 ± 0.002	76040 ± 16	9.428 ± 0.002	76,040 ± 17	9.421 ± 0.002	75983 ± 16
1/2	1	9.469 ± 0.002	76369 ± 16	9.467 ± 0.002	76356 ± 17	9.466 ± 0.002	76349 ± 17
3/2	1	9.526 ± 0.002	76836 ± 17	9.525 ± 0.002	76823 ± 19	9.524 ± 0.002	76819 ± 18
1/2	2	9.565 ± 0.002	77149 ± 18	9.568 ± 0.002	77167 ± 18	9.564 ± 0.003	77139 ± 21
3/2	2	9.625 ± 0.002	77630 ± 17	9.622 ± 0.002	77603 ± 19	9.620 ± 0.003	77588 ± 20
1/2	3	9.663 ± 0.002	77937 ± 17	9.661 ± 0.002	77924 ± 18	9.658 ± 0.002	77895 ± 18
3/2	3	9.721 ± 0.002	78408 ± 17	9.721 ± 0.002	78408 ± 16	9.715 0.003	78355 ± 21
1/2	4	9.761 ± 0.003	78725 ± 20	9.758 ± 0.003	78700 ± 28	9.756 ± 0.005	78689 ± 43
3/2	4	9.817 ± 0.002	79182 ± 17	9.818 ± 0.002	79190 ± 17	9.815 ± 0.002	79160 ± 20
1/2	5	9.852 ± 0.002	79462 ± 19	9.852 ± 0.002	79458 ± 19	9.858 ± 0.007	79513 ± 56
3/2	5	9.918 ± 0.002	79992 ± 17	9.915 ± 0.003	79872 ± 23	9.903 ± 0.002	79875 ± 19
1/2	6	9.949 ± 0.002	80240 ± 17	9.944 ± 0.002	80201 ± 16	9.938 ± 0.002	80159 ± 17
3/2	6	10.010 ± 0.003	80739 ± 21	10.007 ± 0.003	80715 ± 26	10.003 ± 0.002	80677 ± 18
1/2	7	10.044 ± 0.002	81014 ± 17	10.031 ± 0.002	80909 ± 18	10.034 ± 0.002	80933 ± 18
3/2	7	10.101 ± 0.002	81473 ± 16	10.100 ± 0.003	81465 ± 26	10.090 ± 0.002	81385 ± 16
1/2	8	10.135 ± 0.002	81747 ± 16	10.130 ± 0.002	81707 ± 17	10.125 ± 0.002	81667 ± 17
3/2	8	10.191 ± 0.002	82199 ± 16	10.187 ± 0.004	82167 ± 33	10.181 ± 0.002	82118 ± 19
1/2	9	10.227 ± 0.002	82490 ± 17	10.225 ± 0.002	82473 ± 16	10.214 ± 0.002	82385 ± 18
3/2	9	10.284 ± 0.002	82949 ± 16	10.280 ± 0.002	82917 ± 18	10.272 ± 0.002	82852 ± 16
1/2	10	10.316 ± 0.002	83207 ± 16	10.315 ± 0.002	83199 ± 17	10.301 ± 0.002	83086 ± 16
3/2	10	10.375 ± 0.002	83683 ± 16	10.369 ± 0.002	83635 ± 20	10.359 ± 0.002	83554 ± 16
1/2	11	10.405 ± 0.002	83925 ± 16	10.399 ± 0.002	88877 ± 18	10.389 ± 0.002	83796 ± 16
3/2	11	10.463 ± 0.002	84393 ± 17	10.460 ± 0.005	84369 ± 43	10.451 ± 0.002	84296 ± 17
1/2	12	10.495 ± 0.002	84651 ± 17	10.498 ± 0.002	84675 ± 17	10.475 ± 0.003	84490 ± 20
3/2	12	10.554 ± 0.002	85127 ± 17	10.548 ± 0.005	85079 ± 48	10. 535 ± 0.002	84974 ± 17

more favorable for different cation equilibrium distances, as seen in other systems [44]. Indeed, the first autoionization features—converging towards the $a^4\Pi_u$ ionic state—are seen in Fig. 2 to begin at 10.1 eV, which coincides with the departure from the Franck-Condon behavior observed in the TPES of Fig. 3. This explanation likewise applies to the appearance of peaks belonging to the $X^2\Pi_{3/2}(v = 16)$, $X^2\Pi_{1/2}(v = 18)$ and $X^2\Pi_{3/2}(v = 18)$ levels between 10.9 and 11.1 eV in the TPES, which coincides with the first autoionizing feature converging to the $b^4\Sigma_g^-$ ionic state.

3.3.2. S_2^+ excited states

The TPES of S_2 from 11.5 to 15.0 eV is presented in Figs. 5 and 6 along with assignments corresponding to the final cationic states of S_2^+. The assigned spectroscopic parameters are presented in Table 5. Above 12.0 eV, we expected to see the spectral fingerprints of the $A^2\Pi_u$ state (akin to Dyke *et al.*) but the threshold electron signal used to make up the TPES was not strong enough to resolve it and thus our TPES forbids vibrational assignment of the $A^2\Pi_u$ state.

Further comparison with the recorded PES from Dyke *et al.* does

Table 4
Spectroscopic parameters pertaining to the two SO components of the $X^2\Pi_{\Omega,g}$ ground state of S_2^+ and its isotopologues as obtained by including all of the observed vibrational levels.

$X^2\Pi_g$	T_e [cm^{-1}]	ω_e[cm^{-1}]	$\omega_e x_e$[cm^{-1}]	Ref.
$^{32}S_2$	75400 ± 30	807 ± 5	3.88 ± 0.03	This work
		806.099	3.3971	[23]
		805.9	3.38	[21]
$^{33}S^{32}S$	75410 ± 35	797 ± 7	3.5 ± 0.3	This work
$^{34}S^{32}S$	75380 ± 35	805 ± 7	4.7 ± 0.4	This work

show the significantly improved resolution on the $a^4\Pi_u$ state as the quartet splitting of the $a^4\Pi_u$, state ($\Omega = 1/2, 3/2, 5/2$) is clearly visible. Dyke *et al.* predicted a spin–orbit splitting of approximately 160 cm^{-1} or 20 meV. Here, we observe an average splitting of 98 ± 26 cm^{-1} (12.1 ± 3.2 meV) which is well below the resolution of the apparatus used by Dyke *et al.*

In Fig. 6, we see clear signatures of the $b^4\Sigma_g^-$, and $B^2\Sigma_g^-$ states. Between the $b^4\Sigma_g^-$, and $B^2\Sigma_g^-$ states there are several weak peaks that remain unassigned. In the case O_2^+, there are two ionic states found between the $^4\Sigma_g^-$ and the $^2\Sigma_g^-$, namely $^2\Phi_u$ and $^2\Delta_g$ [45]. Indeed, some states are expected to have small oscillator strength coefficients ($f >$

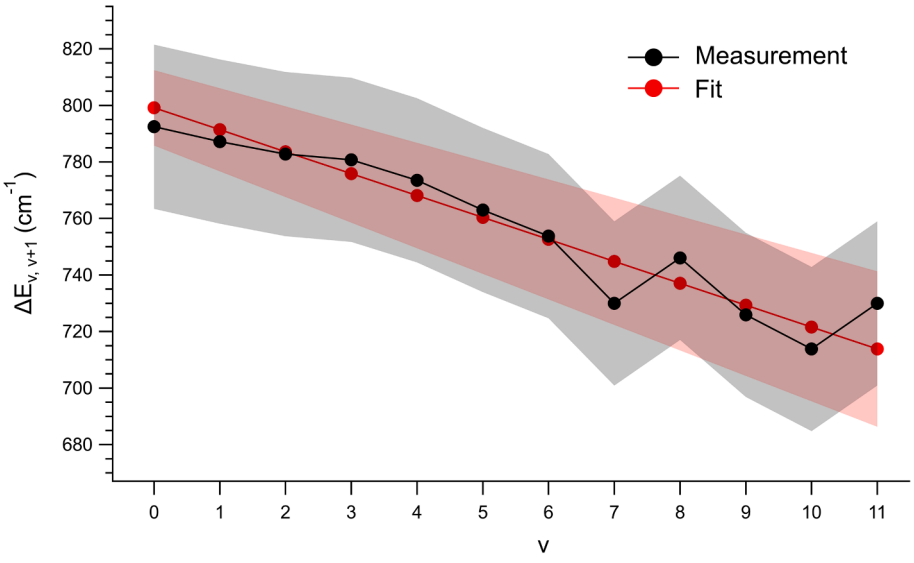

Fig. 4. Vibrational energy level spacings for the $X^2\Pi_{\Omega,g}$ ground state are plotted in black. The red line represents the energy level spacing calculated from the fitted parameters presented in Table 3. Shaded regions denote the propagated uncertainties from the TPES for the measurement (black), and the propagated uncertainties from the fitted parameters (red).

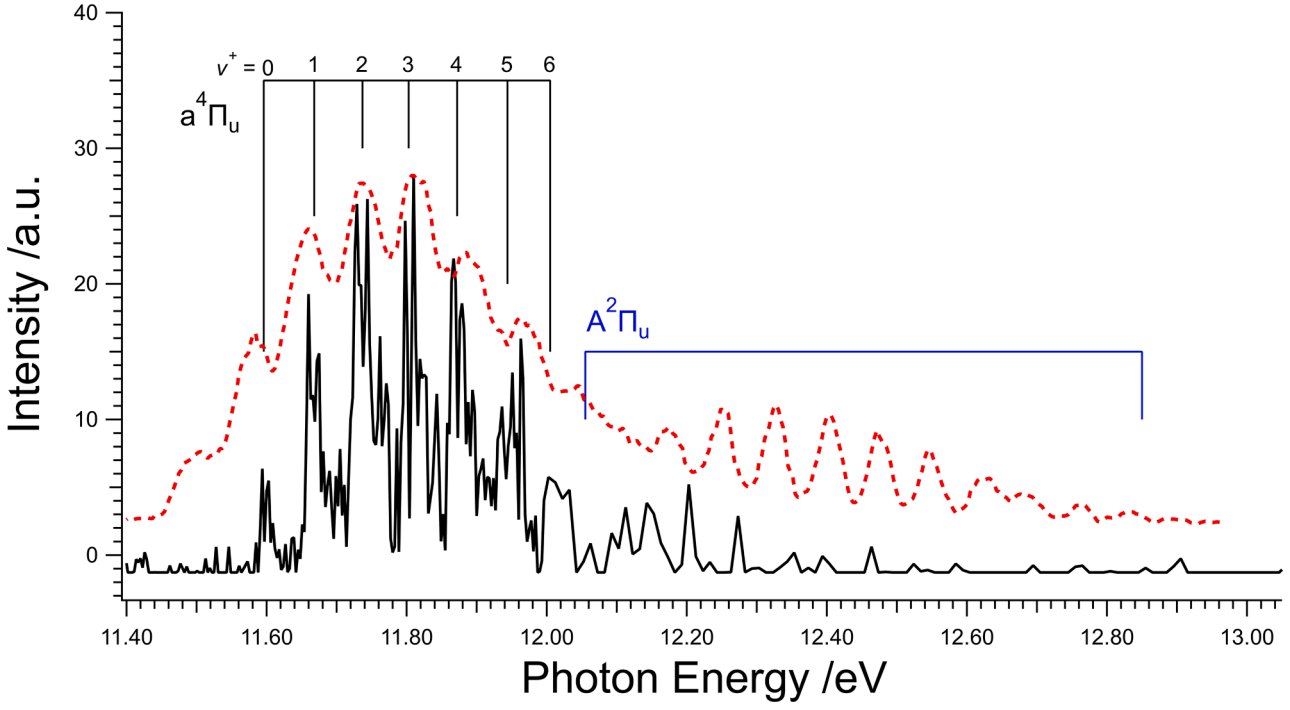

Fig. 5. TPES of S_2 from 11.4 eV up to 12.9 eV. Up to 12.0 eV the step size of the TPES is 3 meV, changing to 10 meV above 12.0. Band assignments of the $a^4\Pi_u$, $A^2\Pi_u$ states are depicted as well as comparison with the PES from Dyke *et al.*[17]

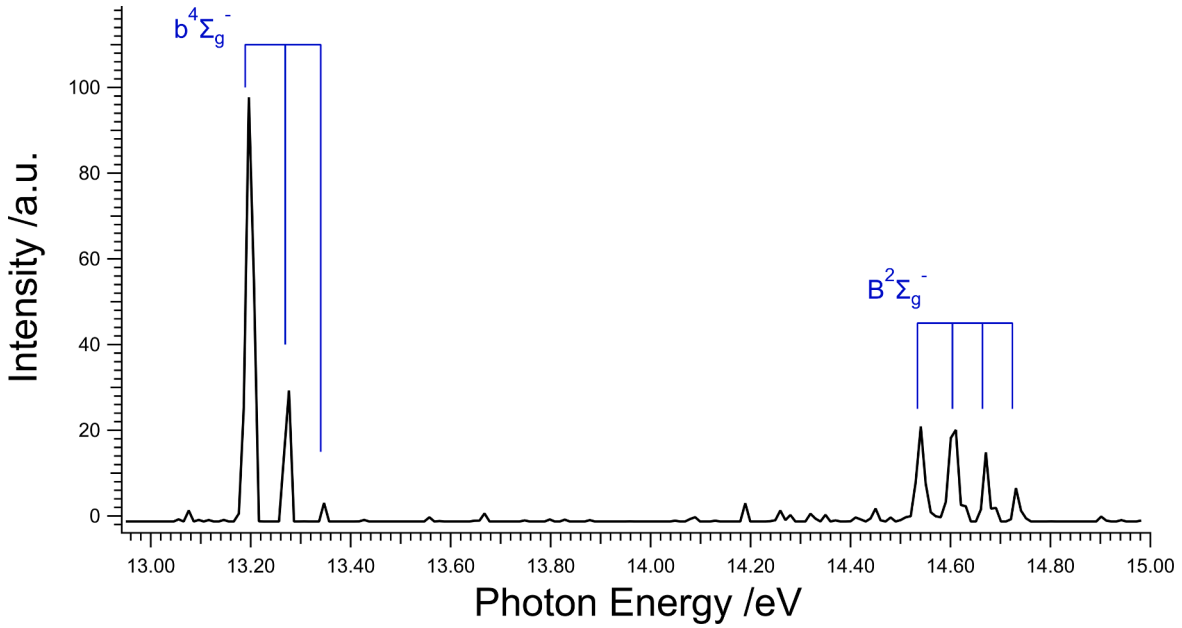

Fig. 6. TPES of S_2 from 13.0 eV up to 14.9 eV. Band assignments of the $b^4\Sigma_g^-$, and $B^2\Sigma_g^-$ states are depicted. Unassigned peaks are denoted with asterisks.

Table 5
Spectroscopic parameters pertaining to the observed excited states of the S_2^+ cation in the TPES. Here, T_e and ω_e (and $\omega_e x_e$ in the case of $B^2\Sigma_g^-$) were fitted to the observed line positions in accordance with $E = T_e + \omega_e(v+½) - w_e x_e(v+½)^2$. E_0 is the excitation energy of the ionic states from the $X^2\Pi_{\Omega,g}$ ground state.

	T_e [cm^{-1}]	E_0 [cm^{-1}]	ω_e [cm^{-1}]	$\omega_e x_e$ [cm^{-1}]	Ref.
$a^4\Pi_u$	93520 ± 30	18470 ± 30	550 ± 10	–	This work
		19438	620		[17]
$A^2\Pi_u$	96950 ± 50	21550 ± 50	-	-	This work
		23551	547	3.1	[17]
$b^4\Sigma_g^-$	106580 ± 30	31770 ± 30	608 ± 20		This work
		30568	581		[17]
$B^2\Sigma_g^-$	117420 ± 30	42440 ± 30	508 ± 20	20 ± 6	This work
		42021	546		[17]

0.01), but may be weakly allowed by couplings with other states and thus show up as very faint signals in our recorded TPES. Another possibility is that these belong to one of the excited states calculated by Yu *et al.* [27] but without a clear spectral pattern, these peaks remain unassigned for now.

4. Summary and conclusions

In light of recent progress on explaining the abundances (or lack thereof) of observed sulfur in the universe, we have investigated the photoionization spectroscopy and dynamics of the sulfur dimer, S_2. These include the first threshold photoelectron spectrum of S_2 whose resolution is significantly improved as compared with previous photoelectron spectra [17]. We also collected the total ion yield of S_2^+ with significantly higher resolution than previous measurements [26]. The high-resolution TPES allows us to fit spectroscopic constants to the ionic states of S_2^+ with higher accuracy and, in turn, guides the assignment of the very rich total ion yield curve exhibiting numerous autoionization features. Interestingly, these autoionization processes also lead to a more precise mapping of the potential energy surface of the $X^2\Pi_{\Omega,g}$ground cation state because highly excited vibrational states on the cation can now be accessed indirectly via Rydberg states.

Some unexplored features in the TPES are still observed around the $b^4\Sigma_g^-$ and the $B^2\Sigma_g^-$ excited states of the cation. These could be due to *e.g.*, other excited states that have been predicted at higher energies [27], hot bands or even ionization of metastable states of neutral S_2.

CRediT authorship contribution statement

Helgi Rafn Hrodmarsson: Data curation, Formal analysis, Investigation, Writing – review & editing,**Gustavo A. Garcia:**Data curation, Methodology, Investigation,**Laurent Nahon:**Project administration, Investigation,**Jean-Christophe Loison:**Data curation, Methodology, Investigation,**Bérenger Gans:**Data curation, Formal analysis, Investigation.

Declaration of Competing Interest

The authors declare that they have no known competing financial interests or personal relationships that could have appeared to influence the work reported in this paper.

Acknowledgments

We warmly thank the whole SOLEIL staff for running smoothly the facility under project 99180002. We are indebted to JF Gil for his help on the SAPHIRS chamber. We also thank Prof. J. Liévin for very constructive discussions. The research described in this work has received financial support from the French Agence Nationale de la Recherche (ANR) under Grant No. ANR-12-BS08-0020-02 (project SYNCHROKIN). H. R. H. is grateful for support from the Marie Sklodowska Curie Actions, proposal ID: 838372.

Appendix A. Supplementary material

Supplementary data to this article can be found online at https://doi.org/10.1016/j.jms.2021.111533.

References

[1] S. Black, The Biochemistry of Sulfur-Containing Compounds, Annu. Rev. Biochem. 32 (1) (1963) 399–418, https://doi.org/10.1146/annurev.bi.32.070163.002151.
[2] E.B. Jenkins, A Unified Representation of Gas-Phase Element Depletions in the Interstellar Medium, ApJ. 700 (2) (2009) 1299–1348, https://doi.org/10.1088/0004-637X/700/2/1299.

[3] M.F. Ahearn, D.G. Schleicher, P.D. Feldman, The discovery of S_2 in comet IRAS-Araki-Alcock 1983d, ApJ. 274 (1983) L99, https://doi.org/10.1086/184158.

[4] S.J. Kim, M.F. A'Hearn, D.D. Wellnitz, R. Meier, Y.S. Lee, The rotational structure of the B-X system of sulfur dimers in the spectra of Comet Hyakutake (C/1996 B2), Icarus 166 (1) (2003) 157–166, https://doi.org/10.1016/j.icarus.2003.07.003.

[5] K. Noll, M. McGrath, L. Trafton, S. Atreya, J. Caldwell, H. Weaver, R. Yelle, C. Barnet, S. Edgington, HST spectroscopic observations of Jupiter after the collision of comet Shoemaker-Levy 9, Science 267 (5202) (1995) 1307–1313, https://doi.org/10.1126/science:7871428.

[6] J.R. Spencer, K.L. Jessup, M.A. McGrath, G.E. Ballester, R. Yelle, Discovery of Gaseous S_2 in Io's Pele Plume, Science 288 (2000) 1208–1210, https://doi.org/10.1126/science.288.5469.1208.

[7] K.L. Jessup, J. Spencer, R. Yelle, Sulfur volcanism on Io, Icarus 192 (1) (2007) 24–40, https://doi.org/10.1016/j.icarus.2007.06.025.

[8] K. Zahnle, M.S. Marley, R.S. Freedman, K. Lodders, J.J. Fortney, Atmospheric Sulfur Photochemistry on Hot Jupiters, ApJ. 701 (2009) L20–L24, https://doi.org/10.1088/0004-637X/701/1/L20.

[9] J.C. Laas, P. Caselli, Modeling sulfur depletion in interstellar clouds, A&A. 624 (2019) A108, https://doi.org/10.1051/0004-6361/201834446.

[10] T.H.G. Vidal, J.-C. Loison, A.Y. Jaziri, M. Ruaud, P. Gratier, V. Wakelam, On the reservoir of sulphur in dark clouds: chemistry and elemental abundance reconciled, MNRAS 469 (2017) 435–447, https://doi.org/10.1093/mnras/stx828.

[11] L.F. Rodríguez-Almeida, I. Jiménez-Serra, V.M. Rivilla, J. Martín-Pintado, S. Zeng, B. Tercero, P. de Vicente, L. Colzi, F. Rico-Villas, S. Martín, M.A. Requena-Torres, Thiols in the Interstellar Medium: First Detection of HC(O)SH and Confirmation of C_2H_5SH, ApJL. 912 (2021) L11, https://doi.org/10.3847/2041-8213/abf7cb.

[12] J. Cernicharo, C. Cabezas, M. Agúndez, B. Tercero, J.R. Pardo, N. Marcelino, J. D. Gallego, F. Tercero, J.A. López-Pérez, P. de Vicente, TMC-1, the starless core sulfur factory: Discovery of NCS, HCCS, H_2CCS, H_2CCCS, and C_4S and detection of C_5S, A&A. 648 (2021) L3, https://doi.org/10.1051/0004-6361/202140642.

[13] J. Cernicharo, C. Cabezas, Y. Endo, N. Marcelino, M. Agúndez, B. Tercero, J. D. Gallego, P. de Vicente, Space and laboratory discovery of HC_3S^+, A&A. 646 (2021) L3, https://doi.org/10.1051/0004-6361/202040013.

[14] M. Agúndez, N. Marcelino, J. Cernicharo, M. Tafalla, Detection of interstellar HCS and its metastable isomer HSC: new pieces in the puzzle of sulfur chemistry, A&A. 611 (2018) L1, https://doi.org/10.1051/0004-6361/201832743.

[15] J. Cernicharo, B. Lefloch, M. Agúndez, S. Bailleux, L. Margulès, E. Roueff, R. Bachiller, N. Marcelino, B. Tercero, C. Vastel, E. Caux, Discovery of the Ubiquitous Cation NS^+ in Space Confirmed by Laboratory Spectroscopy, The Astrophysical Journal Letters. 853 (2018) L22, https://doi.org/10.3847/2041-8213/aaa83a.

[16] C.N. Shingledecker, T. Lamberts, J.C. Laas, A. Vasyunin, E. Herbst, J. Kaestner, P. Caselli, Efficient Production of S_8 in Interstellar Ices: The effects of cosmic ray-driven radiation chemistry and non-diffusive bulk reactions, ApJ. 888 (2020) 52, https://doi.org/10.3847/1538-4357/ab5360.

[17] J.M. Dyke, L. Golob, N. Jonathan, A. Morris, Vacuum ultraviolet photoelectron spectroscopy of transient species. Part 5.—The $S_2(^3\Sigma_g^-)$ molecule | Semantic Scholar, J. Chem. Soc., Faraday Trans. 71 (0) (1975) 1026–1036, https://doi.org/10.1039/F29757101026.

[18] J. Berkowitz, PES of high temperature vapors. VII. S_2 and Te_2, J. Chem. Phys. 62 (10) (1975) 4074–4079, https://doi.org/10.1063/1.430283.

[19] M. Tsuji, I. Murakami, Y. Nishimura, A new emission produced from sulfur monochloride in a helium afterglow: $S_2^+(A^2\Pi_u\text{-}X^2\Pi_g)$, Chem. Phys. Lett. 75 (1980) 536–539, https://doi.org/10.1016/0009-2614(80)80572-0.

[20] M. Tsuji, I. Murakami, Y. Nishimura, UV and visible emission produced from S_2Cl_2 in the rare gas flowing afterglow, J. Chem. Phys. 75 (1981) 5373–5380, https://doi.org/10.1063/1.441982.

[21] A.J. Capel, J.H.D. Eland, R.F. Barrow, Rotational analysis of the A—X bands of S_2^+, Chem. Phys. Lett. 82 (3) (1981) 496–500, https://doi.org/10.1016/0009-2614(81)85427-9.

[22] W. Rosinger, M. Grade, W. Hirschwald, Electron Impact Induced Excitation Processes Involving the Sulfur Clusters S_2 to S_8, Berichte Der Bunsengesellschaft Für Physikalische, Chemie. 87 (6) (1983) 536–542, https://doi.org/10.1002/bbpc.19830870616.

[23] K. Brabaharan, J.A. Coxon, Rotational analysis of the $A^2\Pi_u \rightarrow X^2\Pi_g$ system of $^{32}S_2^+$, J. Mol. Spectrosc. 128 (2) (1988) 540–553, https://doi.org/10.1016/0022-2852(88)90169-5.

[24] C.-C. Zen, Y.-P. Lee, J.F. Ogilvie, Spectra of the vibronic transition A-X of S_2^+ in solid neon, Spectrochim. Acta Part A Mol. Biomol. Spectrosc. 52 (13) (1996) 1727–1735, https://doi.org/10.1016/S0584-8539(96)01734-5.

[25] V.I. Gerasimova, Y.S. Zavorotny, A.O. Rybaltovskii, P.V. Chernov, O.D. Sazhin, R. R. Khrapko, A.A. Frolov, Color Centers in Sulfur-Doped Silica Glasses: Spectroscopic Manifestations of an S_2^+ Interstitial Molecular Ion, Glass Phys. Chem 28 (2002) 5–10, https://doi.org/10.1023/A:1014241211374.

[26] C.L. Liao, C.Y. Ng, Molecular beam photoionization study of S_2, J. Chem. Phys. 84 (2) (1986) 778–782, https://doi.org/10.1063/1.450576.

[27] W. Yu, Z. Zhu, C. Chuncai, S. Deheng, A theoretical investigation of the S_2^+ cation in the gas phase, Can. J. Chem. (2014), https://doi.org/10.1139/cjc-2014-0255.

[28] L.R. Varas, L.H. Coutinho, R.B. Bernini, A.M. Betancourt, C.E.V. de Moura, A. B. Rocha, G.G.B. de Souza, Breaking the disulfide chemical bond using high energy photons: the dimethyl disulfide and methyl propyl disulfide molecules, RSC Adv. 7 (2017) 36525–36532, https://doi.org/10.1039/C7RA05001A.

[29] T. Baer, R.P. Tuckett, Advances in threshold photoelectron spectroscopy (TPES) and threshold photoelectron photoion coincidence (TPEPICO), Phys. Chem. Chem. Phys. 19 (15) (2017) 9698–9723, https://doi.org/10.1039/C7CP00144D.

[30] L. Nahon, N. de Oliveira, G.A. Garcia, J.-F. Gil, B. Pilette, O. Marcouille, B. Lagarde, F. Polack, DESIRS: a state-of-the-art VUV beamline featuring high resolution and variable polarization for spectroscopy and dichroism at SOLEIL, Journal of Synchrotron Radiation. 19 (2012) 508–520, https://doi.org/10.1107/S0909049512010588.

[31] X. Tang, G.A. Garcia, J.-F. Gil, L. Nahon, Vacuum upgrade and enhanced performances of the double imaging electron/ion coincidence end-station at the vacuum ultraviolet beamline DESIRS, Rev. Sci. Instrum. 86 (2015), https://doi.org/10.1063/1.4937624.

[32] G.A. Garcia, B.K.C. de Miranda, M. Tia, S. Daly, L. Nahon, DELICIOUS III: A multipurpose double imaging particle coincidence spectrometer for gas phase vacuum ultraviolet photodynamics studies, Rev. Sci. Instrum. 84 (2013), https://doi.org/10.1063/1.4807751.

[33] B. Mercier, M. Compin, C. Prevost, G. Bellec, R. Thissen, O. Dutuit, L. Nahon, Experimental and theoretical study of a differentially pumped absorption gas cell used as a low energy-pass filter in the vacuum ultraviolet photon energy range, Journal of Vacuum Science & Technology A-Vacuum Surfaces and Films. 18 (2000) 2533–2541, https://doi.org/10.1116/1.1288196.

[34] O. Marcouille, P. Brunelle, O. Chubar, F. Marteau, M. Massal, L. Nahon, K. Tavakoli, J. Veteran, J.-M. Filhol, Design, construction and magnetic measurements of the HU640 (OPHELIE2) undulator dedicated to the DESIRS VUV beamline at SOLEIL, in: Choi, JY and Rah, S (Ed.), Synchrotron Radiation Instrumentation Pts 1 & 2, American Institute of Physics, 2 Huntington Quadrangle, Ste 1No1, Melville, NY 11747-4501 USA, 2007, pp. 311.

[35] G.A. Garcia, X. Tang, J.-F. Gil, L. Nahon, M. Ward, S. Batut, C. Fittschen, C. A. Taatjes, D.L. Osborn, J.-C. Loison, Synchrotron-based double imaging photoelectron/photoion coincidence spectroscopy of radicals produced in a flow tube: OH and OD, J. Chem. Phys. 142 (16) (2015) 164201, https://doi.org/10.1063/1.4918634.

[36] H.R. Hrodmarsson, G.A. Garcia, L. Nahon, J.-C. Loison, B. Gans, The absolute photoionization cross section of the mercapto radical (SH) from threshold up to 15.0 eV, Phys. Chem. Chem. Phys. 21 (46) (2019) 25907–25915, https://doi.org/10.1039/C9CP05809E.

[37] G.A. Garcia, L. Nahon, I. Powis, Two-dimensional charged particle image inversion using a polar basis function expansion, Rev. Sci. Instrum. 75 (11) (2004) 4989–4996, https://doi.org/10.1063/1.1807578.

[38] H.R. Hrodmarsson, G.A. Garcia, L. Nahon, B. Gans, J.-C. Loison, Threshold Photoelectron Spectrum of the Anilino Radical, The Journal of Physical Chemistry A. 123 (42) (2019) 9193–9198, https://doi.org/10.1021/acs.jpca.9b0727310.1021/acs.jpca.9b07273.s001.

[39] H.R. Hrodmarsson, J.-C. Loison, U. Jacovella, D.M.P. Holland, S. Boyé-Péronne, B. Gans, G.A. Garcia, L. Nahon, S.T. Pratt, Valence-Shell Photoionization of C4H5: The 2-Butyn-1-yl Radical, J. Phys. Chem. A 123 (8) (2019) 1521–1528, https://doi.org/10.1021/acs.jpca.8b11809.

[40] E. Lindholm, Rydberg Series in Small Molecules.i. Quantum Defects in Rydberg Series, Arkiv for Fysik. 40 (1969) 97-.

[41] K. Yoshino, Y. Tanaka, Absorption spectrum of krypton in the vacuum uv region, J. Opt. Soc. Am. 69 (1979) 159, https://doi.org/10.1364/JOSA.69.000159.

[42] K. Yoshino, Absorption Spectrum of the Argon Atom in the Vacuum-Ultraviolet Region, J. Opt. Soc. Am. 60 (1970) 1220, https://doi.org/10.1364/JOSA.60.001220.

[43] M.J. Cooper, C.M. Western, Two-colour double resonance multiphoton ionisation spectroscopy of S_2, Chem. Phys. Lett. 267 (3-4) (1997) 365–369, https://doi.org/10.1016/S0009-2614(97)00099-7.

[44] M. Briant, L. Poisson, M. Hochlaf, P. de Pujo, M.-A. Gaveau, B. Soep, Ar_2 Photoelectron Spectroscopy Mediated by Autoionizing States, Phys. Rev. Lett. 109 (2012), 193401, https://doi.org/10.1103/PhysRevLett.109.193401.

[45] F. Merkt, P.M. Guyon, J. Hepburn, High-resolution threshold photoelectron spectrum of molecular oxygen, Chem. Phys. 173 (3) (1993) 479–484, https://doi.org/10.1016/0301-0104(93)80162-3.